Applied Geochemistry 129 (2021) 104955

Contents lists available at ScienceDirect

Applied Geochemistry

journal homepage: http://www.elsevier.com/locate/apgeochem

Evaluating feedstocks for carbon dioxide removal by enhanced rock weathering and CO_2 mineralization

Carlos Paulo [a,*], Ian M. Power [a], Amanda R. Stubbs [a], Baolin Wang [b], Nina Zeyen [b], Siobhan A. Wilson [b]

[a] Trent School of the Environment, Trent University, Peterborough, Ontario, K9L 0G2, Canada
[b] Department of Earth and Atmospheric Sciences, University of Alberta, Edmonton, Alberta, T6G 2E3, Canada

ARTICLE INFO

Editorial handling by Prof. M. Kersten

Keywords:
Easily extractable cations
CO_2 mineralization
Enhanced rock weathering
Carbon dioxide removal
Carbonation feedstock

ABSTRACT

Mineralogically complex feedstocks, including kimberlite, serpentinite, and wollastonite skarns, have vast capacities to sequester carbon dioxide (CO_2) through enhanced rock weathering and CO_2 mineralization. However, only a small reactive fraction of these feedstocks will be accessible for carbon dioxide removal at Earth's surface conditions. We have developed a new method to evaluate the reactivity of mineral feedstocks that consists of a batch leach test using CO_2 coupled with total inorganic carbon (TIC) analysis to quantify easily extractable Mg and Ca from non-carbonate (desirable) cation sources. Kimberlite residues from the Venetia Diamond Mine (South Africa), serpentinites, wollastonite skarn, and brucite ore were tested and the results were compared to those from commercial ammonium acetate (NH_4OAc) leach tests. A strong correlation ($R^2 = 0.99$) between leached Ca and TIC showed that carbonate minerals (e.g., calcite in kimberlite) are a substantial and undesirable source of easily extractable cations that must be excluded in calculating CO_2 sequestration potential. Silicate dissolution (e.g., serpentine) was inferred from the strong positive correlation ($R^2 = 0.94$) between Mg and Si concentrations leached from kimberlites and serpentinites. Strong correlations between leached Ca and Si were only detected for wollastonite skarns, whereas Mg leaching from samples with high abundances of brucite showed weak or no relationship to TIC or Si. The ability to distinguish between sources (non-carbonate versus carbonate) of easily extractable cations is necessary to accurately assess CO_2 sequestration potential. The maximum CO_2 storage capacity of the Venetia kimberlites was 268–342 kg CO_2/t, and our leach test estimated an accessible potential in the range of 3–9 kg CO_2/t when only accounting for non-carbonate sources. Our CO_2 batch leach test is useful to evaluate the reactivity of mineralogically complex feedstocks at Earth's surface conditions for the purpose of carbon dioxide removal.

1. Introduction

The global effort to mitigate the impacts of climate change will require the adoption of strategies and technologies to decarbonize various industrial sectors, as well as to remove greenhouse gas (GHG) from the atmosphere (IPCC, 2018; Minx et al., 2018). A drastic reduction of worldwide GHG emissions is desirable to limit the increase of global mean temperature (<1.5 °C) and to keep atmospheric carbon dioxide (CO_2) levels <490 ppm before irreversible changes are introduced to Earth systems (IPCC, 2019). To fulfill this goal, it is imperative that negative emissions technologies (NETs) that remove and sequester atmospheric CO_2 are rapidly adopted (Daval, 2018; IPCC, 2018; 2019; Minx et al., 2018; Pogge von Strandmann et al., 2019). Moreover, the integration of NETs in industrial-scale projects can help achieve local and global policy targets to promote decarbonization, as well as to create positive socio-economic impacts in communities (Fajardy et al., 2019; Haszeldine et al., 2018; IPCC, 2018).

Enhanced rock weathering (ERW) and CO_2 mineralization comprise various approaches to sequestering CO_2 as either a dissolved or solid phase (National Academies of Sciences, 2019; Power et al., 2013a). These approaches rely on accelerated dissolution (weathering) of alkaline earth silicate and hydroxide minerals and subsequent release of calcium and magnesium to precipitate as carbonate minerals (Assima et al., 2014b; Daval, 2018; Kirchofer et al., 2013; National Academies of Sciences, 2019; Veetil and Hitch, 2020). Several mineral and rock feedstocks are available, including olivine (e.g. Oelkers et al., 2018),

* Corresponding author.
E-mail address: cfernandesesilvapaul@trentu.ca (C. Paulo).

https://doi.org/10.1016/j.apgeochem.2021.104955
Received 29 October 2020; Received in revised form 18 February 2021; Accepted 1 April 2021
Available online 6 April 2021

serpentine group minerals (e.g. Assima et al., 2014a; Thom et al., 2013), wollastonite (e.g. Daval et al., 2009; Di Lorenzo et al., 2018; Haque et al., 2020; Haque et al., 2019), brucite (e.g. Harrison et al., 2013), basalt (e.g. Oelkers et al., 2008), peridotite (e.g. Kremer et al., 2019), and kimberlite (e.g. Mervine et al., 2018; Wilson et al., 2011). In addition, different types of industrial alkaline wastes such as steel slag, concrete wastes, and ultramafic mine tailings have the advantage of being easily accessible (Baena-Moreno et al., 2019; Kirchofer et al., 2013; Power et al., 2013a; Renforth, 2019). In particular, mine wastes can be an ideal resource for ERW and CO_2 mineralization since most of the costs linked to comminution are largely reduced due to ore processing (Li et al., 2018).

Recent studies have demonstrated that weathering of mineral feedstocks at low-temperature conditions may be feasible through *ex-situ* and *in-situ* processes that accelerate carbon mineralization reactions. These processes include using higher CO_2 partial pressures, the pre-treatment of materials subject to CO_2 mineralization (physical or chemical treatment), the utilization of mineral feedstocks as soil amendments, or even feedstock carbonation and carbonate precipitation via microbial processes (Daval, 2018; Hamilton et al., 2020; Haque et al., 2020; Haque et al., 2019; Li et al., 2018; McCutcheon et al., 2017; Pogge von Strandmann et al., 2019; Power et al., 2013b). Alkaline wastes, including mine residues, have in common their high magnesium and/or calcium content in the form of silicate and hydroxide minerals or amorphous phases (e.g., glass) that can chemically bind to CO_2 (Assima et al., 2014a; Renforth, 2019; Sanna et al., 2014b). In general, rapid extraction of divalent cations (e.g., Mg^{2+} and Ca^{2+}) via mineral dissolution is highly desirable (Assima et al., 2014a; Bonfils et al., 2012; Vanderzee et al., 2019). These cations are rapidly leached from reactive phases and mineral surfaces during transient dissolution and correspond to the easily extractable cations or labile cations fraction of the feedstock (Daval et al., 2013; Power et al., 2020; Vanderzee et al., 2019).

Cation release is controlled by mineral chemistry and physical properties along with solution chemistry, and tends to be slower at low temperature and pressure conditions (Schott et al., 2009; Zhao et al., 2010). As a result, CO_2 mineralization reactions are often limited by cation supply at low temperature and pressure conditions rather than by CO_2 supply or carbonate precipitation (Power et al., 2013a, 2014). This limitation is greater for feedstocks with complex mineralogical assemblages that are dominated by recalcitrant minerals such as silicates. In these cases, the success of CO_2 mineralization technologies depends mostly on the availability of easily extractable cations in highly reactive mineral phases, such as brucite (Power et al., 2020; Vanderzee et al., 2019). Thus, knowing the amount of cations that are easily extractable under specific conditions (e.g., the feedstock reactivity at ambient conditions) is a critical step to assess the feasibility of mineralogically complex feedstocks for CO_2 mineralization and their to potential to offset industrial GHG emissions.

Leaching tests are common laboratory procedures that are used to measure and predict cation release from soils, rocks, or tailings (Davis et al., 2019; Dohrmann, 2006). The minerals industry has adopted these tests as predictive tools to estimate the reactivity of tailings or metals mobility in soils. For example, acid/base accounting (ABA), net acid potential (NAP), and leaching tests have helped the minerals industry to anticipate problems such as acid generation and metal release from mine wastes (INAP, 2009). These tests are routine and essential tools for mine planners to design adequate waste management plans that comply with regulations (Davis et al., 2019). A similar expectation can be made for an analytical tool that can easily predict the mineral feedstock CO_2 mineralization potential using a simple reactivity test. Such a technique could expedite the classification of suitable mineral feedstocks for enhanced rock weathering or CO_2 mineralization projects within mine waste management areas.

Kinetic leaching tests, flow-through leaching experiments, and CO_2 fluxes (e.g., Awoh et al., 2013; Harrison et al., 2015; Kandji et al., 2017; Power et al., 2020) have been used to estimate the CO_2 mineralization potential of mineral feedstocks. Although these methods provide valuable information on the long-term geochemical behaviour of the mineral carbonation feedstock, these are not a rapid and simple analytical method that could be easily adopted as a routine protocol for CO_2 mineralization assessments. Here, we propose a new method to assess the reactivity of mineralogically complex feedstocks (wollastonite skarn, serpentinites, and kimberlite mine wastes) under ambient conditions. This method was designed to measure the easily extractable cations, in particular, Mg and Ca. Batch CO_2 leaches coupled with total inorganic carbon (TIC) analyses were used to quantify cation release from both desirable non-carbonate minerals (e.g., silicates and hydroxides) and undesirable carbonate minerals. This methodology provides a robust, comprehensive, and simple approach for quantifying the CO_2 mineralization potential of mineral feedstocks and evaluating their suitability for carbon dioxide removal.

2. Materials and methods

2.1. Solids characterization

2.1.1. Sample acquisition and preparation

Processed kimberlite mine wastes were sampled at Venetia Diamond Mine (Limpopo Province, South Africa), owned by De Beers Group of Companies to assess the potential for ERW and CO_2 mineralization. Fieldwork was conducted in 2017 and 2018, and samples were collected from the two fine residues deposits (FRDs), one coarse residues deposit (CRD) at Venetia, as well as from the ore stockpiles. These residues were dominated by massive volcanoclastic kimberlite facies. The FRDs have a combined area of approximately 3.5 km^2 with two impoundments that receive the processed fine residues (<1 mm) as a slurry from pipes along their peripheries. A bulk sample of freshly processed fine residues (FRD1) was collected as a slurry from an outlet pipe for comparison to residues that have been already deposited. In addition, a subset of nine samples (FRD2 to FRD10) collected at different depths and locations within the FRD impoundments was characterized and used in experiments (Table 1). Bulk CRD (1–8 mm grain size) samples were obtained from dry stacks in an impoundment with a smaller footprint (~0.5 km^2) and with minimal porewater content. Several dark volcanoclastic kimberlite (DVK) specimens - a dark grey to black carbonatized kimberlite lithofacies from Venetia K01 pipe (Tait and Brown, 2008) - were collected from ore stockpiles. This kimberlite facies was not dominant in previously processed kimberlite, yet is expected to become the major facies in future production at the mine. The rocks were combined, crushed and pulverized in an Essa® LM2 Pulverizing Mill (FLSmith, Copenhagen, Denmark) to sizes comparable to fine residues (<1 mm).

Other mineralogically complex feedstocks were sourced for reactivity tests (Table 1). A wollastonite skarn (wol) sample was acquired as sand-sized soil amendment packages from the Canadian Wollastonite quarry (Ontario, Canada). A sample dominated by brucite (brc) was sourced from the Brucite Mine (Nevada, USA). Three serpentinite samples were obtained from different sites, namely serpentinite (srp1) from the Lizard Complex (Cornwall, United Kingdom), serpentinite (srp2) from Feather River Canyon (California, USA), and serpentinite (srp3) from the Baptiste deposit located within the Decar Nickel District (British Columbia, Canada). Samples of brucite and the wollastonite skarn were obtained as coarse sands, whereas srp1 and srp2 were obtained as rock hand specimens. These feedstocks were crushed and/or pulverized to a finer grain size in line with Venetia fine residues characteristics (<1 mm). The sample of serpentinite (srp3) from the Baptiste deposit was obtained as a pulverized sample.

2.1.2. Particle size and surface area

Particle size distributions were obtained using a Vibratory Sieve Shaker AS 200 Basic (Retsch) and a Horiba LA-950V2 laser scattering particle size distribution analyzer (Teledyne, USA).

Table 1
Sample description, surface area (m^2/g), and summary of geochemistry (wt.% oxide), CO_2 batch leaching (wt.% leached), and NH_4OAc (wt.% leached) results.

Sample	Description	Code	*n*	m^2/g	Geochemistry (%)			CO_2 batch leaching (%)						NH_4OAc (%)		
					CaO	MgO	SiO	Ca	Mg	Si	Na	TIC_i	TIC_L	Ca	Mg	Na
Brucite mine (bru)*	sand-sized soil, pulverized	**brc**	**3**	5.30	1.46	62.80	1.89	0.08	6.59	0.03	0.01	1.22	*n.d*	0.09	<10	0.00
Brucite mine (10%brc)/ SiO_2		**brcQ**	**3**	0.42	*n.d.*	*n.d.*	*n.d.*	0.07	2.71	0.01	0.01	0.11	0.08	n.d.	n.d.	n.d.
Wollastonite skarn (wol) *	sand-sized soil, pulverized	**wol**	**3**	0.90	26.07	6.38	56.37	3.62	0.01	0.47	0.01	0.22	0.10	1.19	0.00	0.00
Wollastonite skarn (10% wol)*/SiO_2		**wolQ**	**2**	*n.d.*	*n.d.*	*n.d.*	*n.d.*	0.53	0.01	0.06	0.01	*n.d.*	<0.01	*n.d.*	*n.d.*	*n.d.*
Serpentinites																
Lizard Complex (srp1)*	rock, pulverized	**srp1**	**3**	25.30	0.03	34.30	38.27	0.02	0.29	0.14	0.03	0.02	0.01	0.01	0.07	0.02
Feather River Canyon (srp2)*	rock, pulverized	**srp2**	**3**	61.14	0.05	37.73	40.80	0.05	0.93	0.42	0.01	0.02	0.01	0.02	0.23	0.01
Baptiste Nickel deposit (srp3)	rock pulverized	**srp3**	**3**	3.05	0.02	42.85	34.65	0.01	3.10	0.09	0.01	0.04	<0.01	0.00	4.04	0.00
Venetia kimberlite																
Unweathered samples																
Dark volcanoclastic kimberlite*	rock pulverized	**DVK**	**3**	18.00	7.77	25.75	38.10	1.12	0.33	0.20	0.38	0.40	0.36	1.56	0.10	0.36
Coarse residue deposits	1–8 mm, dry stacks	**CRD**	**3**	5.80	7.13	21.22	42.22	1.13	0.14	0.08	0.19	0.53	0.07	0.44	0.02	0.17
Bulk fine residue 1	<1 mm, slurry	**FRD1**	**3**	7.67	6.77	22.30	37.90	1.06	0.17	0.12	0.27	0.46	0.14	2.63	0.08	0.50
Weathered samples																
Fine residues 2	<1 mm, 90–125 cm	**FRD2**	**3**	*n.d*	6.87	20.20	41.30	1.42	0.19	0.14	0.61	0.55	0.52	2.63	0.08	0.50
Fine residues 3	<1 mm, 37–45 cm	**FRD3**	**3**	10.70	6.91	21.90	41.90	1.35	0.34	0.19	0.34	0.48	0.39	1.75	0.07	0.35
Fine residues 4	<1 mm, 123–134 cm	**FRD4**	**3**	8.41	6.29	14.00	48.70	1.92	0.27	0.17	0.28	0.64	0.60	2.18	0.08	0.26
Fine residues 5	<1 mm, 26–55 cm	**FRD5**	**3**	11.04	7.09	19.10	40.80	2.27	0.16	0.15	0.62	0.77	0.73	3.31	0.07	0.62
Fine residues 6	<1 mm, 135–162 cm	**FRD6**	**3**	12.47	7.08	19.50	40.90	2.06	0.18	0.12	0.61	0.73	0.70	3.05	0.09	0.63
Fine residues 7	<1 mm, 0–5 cm, crust	**FRD7**	**3**	6.52	6.59	15.10	46.60	1.80	0.20	0.17	0.37	0.58	0.54	2.00	0.05	0.36
Fine residues 8	<1 mm, 53–54 cm	**FRD8**	**3**	12.88	7.10	21.10	41.50	1.72	0.25	0.17	0.41	0.59	0.56	2.38	0.11	0.45
Fine residues 9	<1 mm, 10–15 cm	**FRD9**	**3**	6.55	8.09	19.80	43.90	1.28	0.19	0.15	0.29	0.54	0.40	1.56	0.04	0.26
Fine residues 10	<1 mm, 61–67 cm	**FRD10**	**3**	10.17	7.76	19.30	44.00	1.30	0.19	0.16	0.33	0.46	0.35	1.80	0.04	0.31

n.d.: non-determined. TIC_i: initial TIC. TIC_L: leached TIC.

Brunauer–Emmett–Teller (BET) specific surface areas (Brunauer et al., 1938) were determined by N_2 adsorption. Samples were degassed overnight (200 °C) on a Smart VacPrepTM 067 (Micromeritics, Norcross, GA, USA). BET analysis was performed at 77 K (−196 °C) on the Micromeritics TriStar II Plus adsorption unit (Micromeritics, Norcross, GA, USA), and N_2 isotherms were acquired using a p/p^0 range of 0.01–0.90. All data processing was conducted on MicroActive Interactive software (Micromeritics, Norcross, GA, USA).

2.1.3. Bulk geochemistry

Bulk geochemical analyses were completed using X-ray Fluorescence (XRF) spectroscopy at SGS Canada laboratories (Lakefield, Ontario, Canada). Total inorganic carbon (TIC) was determined using a CO_2 coulometer (CM5017, UIC Inc, USA), which measures the absolute mass of inorganic carbon in a sample. All samples were micronized (7 min) in anhydrous ethanol using a McCrone Micronizing Mill (Retsch Gmbh, Germany) to ensure a complete carbonate reaction. The samples were loaded into 25 mL glass flasks and acidified with 2N H_2SO_4 (10 mL) at 50 °C to dissolve carbonates, and the evolved CO_2 gas was directed to a colorimetric cell. A pre-scrubber solution (KOH 45 v/v%) was used to remove any CO_2 present in the carrier gas (100 mL/min) as well as a post scrubber ($AgNO_3$ 3 v/v%) to remove H_2S, SO_x, and halogens from the gas stream which can form as a result of the sample acidification. The colorimetric cell was partially filled by an aqueous solution containing monoethanolamine mixed with a colorimetric indicator, and two electrodes (platinum and silver). In this method, CO_2 reacts with monoethanolamine to form a titratable acid (hydroxyethylcarbamic acid), and electrochemically generated OH^- in the platinum electrode neutralizes the solution until it returns to its original color or transmittance. The color change is measured as a percent transmittance (%T) by a photodetector. The change is proportional to the concentration of hydroxyethylcarbamic acid formed and, therefore, equivalent to the amount of inorganic carbon injected into the cell. This method is accurate to within a ±1.25% range of results and the detection range is 1–10,000 μg C. Blank and Alfa Aesar calcium carbonate ($CaCO_3$) chelometric standards (99.95–100.05% purity) were analyzed each day the instrument was in use to ensure the accuracy of the readings.

2.1.4. Mineralogy

X-ray diffraction patterns for each feedstock were obtained from micronized samples under the same humidity conditions (20–30%) using a Bruker D8 Advance θ–θ powder X-ray diffractometer equipped with a LYNXEYE XE 1D Position Sensitive Detector in the Environmental Economic Geology Laboratory, University of Alberta. Details on the preparation of samples and data analysis are provided as supplementary information.

2.2. Leaching tests

2.2.1. CO_2 batch leaching

CO_2 batch leaches were conducted in 125 mL polycarbonate flasks with a stir bar and 100 mL of deionized water (18.2 MΩ cm). The batch leach setup was chosen because fine grain material such as processed mine feedstock or rock would not be recovered in a flow-through reactor. The flasks were weighed before each test and placed on a multipoint magnetic stir plate set at 525 rpm (Cimarec™, Telesystem, Thermo Scientific). Dry CO_2 gas was bubbled uninterruptedly into the deionized water through Tygon® tubing (Tygon S3 E−3603 NSF51) using an FM-1050 (E606) flow meter (Matheson, USA) connected to a CO_2 tank (>99%, 10 psi). CO_2 was bubbled through deionized water at

0.12 Standard Liter per Minute (SLPM). After 1 h, waters had reached equilibrium with CO_2 at pH 3.9 as confirmed by geochemical modelling with PHREEQC (Parkhurst and Appelo, 2013). Mineral feedstock samples (0.26 ± 0.01 g) were then mixed into the solutions without the interruption of CO_2 bubbling. All CO_2 leaching tests were run in triplicate at ambient laboratory conditions (~23 °C).

After 48 h, the CO_2 gas bubbling was stopped, and the weight of flasks recorded to account for evaporation that varied between 10% and 26% by mass. Leachate samples were collected with a syringe, filtered (0.22 μm), and acidified (2% v/v HNO_3 for trace analysis, Aristar®, UK). Element analysis was performed by inductively coupled plasma - optical emission spectrometry (ICP-OES) with an Optima 7000 DV (PerkinElmer, USA) with detection limits (MDL) for Ca, Mg, Na, and Si at 0.13, 0.01, 0.05, and 0.06 mg/L, respectively. Blanks and Ca standards (10 ppm Ca standard for ICP, Ricca Chemical, USA) were used to verify the method accuracy.

Suspensions of reacted solids were transferred to 50 mL tubes and centrifuged (Sorvall™ ST 16, Thermo Fisher Scientific) at 21,406×*g* for 45 min. Supernatants were decanted, and the solids were washed in anhydrous ethanol, and then centrifuged to remove water and reduce mineral dissolution or precipitation in the water film surrounding the mineral feedstock particles. This procedure was repeated 3 times. The recovered solids were micronized (McCrone Micronizing Mill, Retsch GmbH, Germany) for 7 min with anhydrous ethanol and dried for total inorganic carbon analysis.

$CaCO_3$ (≥98%, Caledon, Canada) was mixed with quartz (SiO_2) sand (0.1–0.5 mm; Sigma-Aldrich, Germany) in the proportions of 0.7, 1.3, 3.0, 9.0 and 12.0 wt% to calibrate TIC dissolution from solid samples. In addition, a mixture of 90 wt% quartz sand with 10 wt% of the Brucite Mine sample (brcQ) and mixtures with 10 wt% and 13 wt% of the wollastonite sample (wolQ) in quartz were prepared. These diluted mineral feedstocks were necessary for calibration purposes as the case of material recovered from highly reactive samples containing brucite represented less than 60% of the initial sample mass and that resulted in unreliable TIC data. By manipulation of the mass fraction of brucite within a mixture with relatively unreactive quartz, a larger mass of the solids could be recovered from the leachates for TIC analysis.

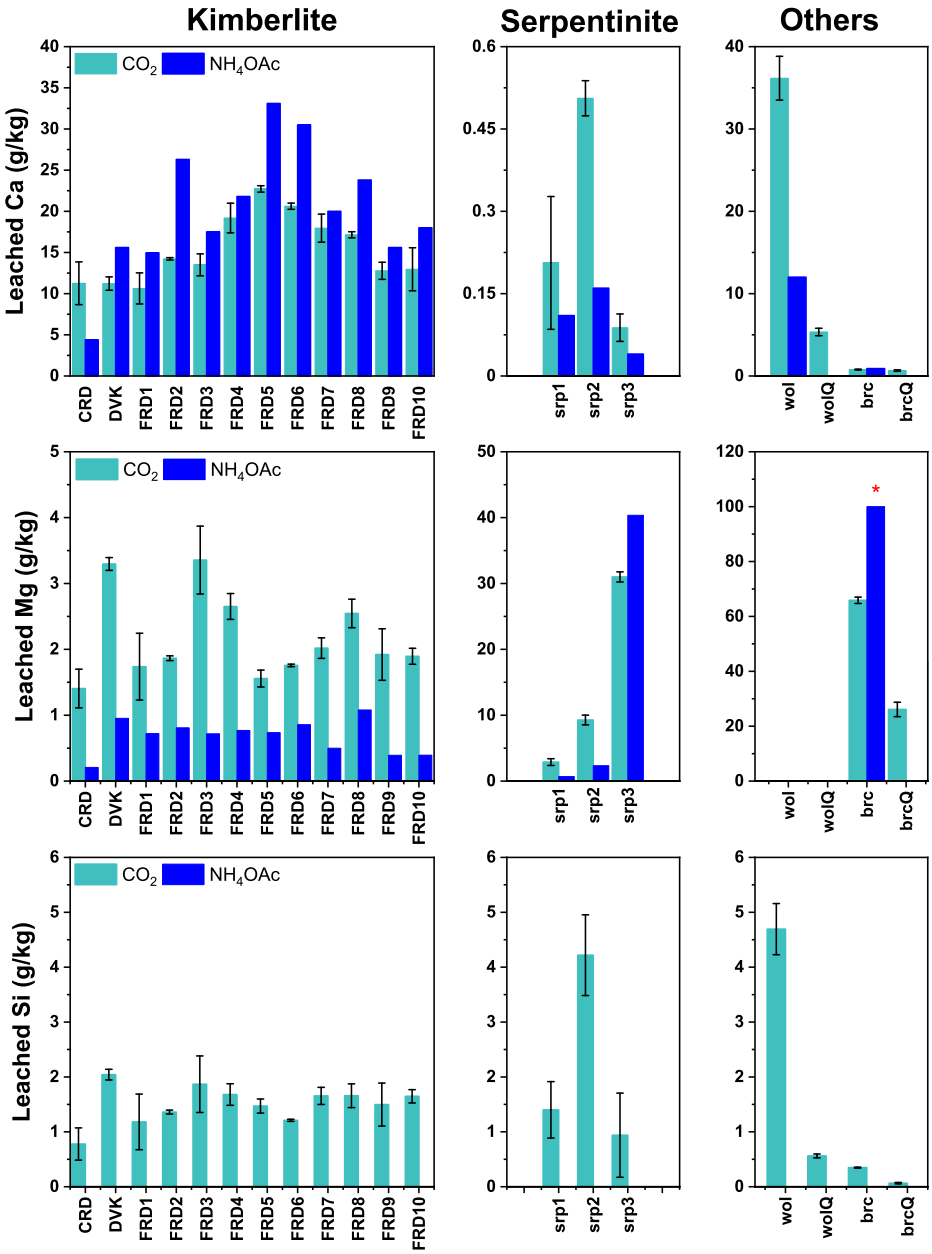

Fig. 1. Comparison between Ca and Mg leached with NH_4OAc (blue) and CO_2 (light blue) methods from Venetia kimberlite residues (CRD, FRD, DVK), serpentinites (srp1, srp2, and srp3), wollastonite skarn (wol and wolQ), and Brucite Mine (brc and brcQ) sample. Concentration units are given as the mass of cation released per mass of the sample in g/kg. CO_2 results are presented as averages (n = 3) with standard deviation error bars for CO_2 batch leaching. NH_4OAc results were obtained only for individual samples for the purpose of comparison to our CO_2 batch leaching test. NH_4OAc data was not obtained for the diluted samples (wolQ and bruQ). Si was only measured for the CO_2 test. The red star indicates that Mg leached from brc (NH_4OAc) exceeded the maximum concentration limit of the analytical method. (For interpretation of the references to color in this figure legend, the reader is referred to the Web version of this article.)

2.2.2. Ammonium acetate leaching

Samples were analyzed by ALS Canada Ltd. (Vancouver, Canada) by ammonium acetate leach (NH_4OAc) to compare to CO_2 batch leaches. The method consisted of leaching 1.0 g of material with 40 mL ammonium acetate solution in acetic acid shaken for 2 h. The final solution is then separated from the solids by centrifuging and decanting the supernatant. Quantification of cations in leachates was done by inductively coupled plasma - mass spectrometry (ICP-MS). Ca, Mg, and Na detection limits were 10, 0.5, 5 mg/L. Si was not measured because samples in the NH_4OAc method are introduced in a borosilicate glass whose dissolution can impact results.

3. Results

3.1. Ca and Mg release from serpentinites, wollastonite skarn, and brucite

The CaO content (Table 1) in the serpentinites was less than 0.1 wt%, and Ca-rich minerals were either absent (srp1 and srp2) or present at trace abundances, such as diopside (0.7 wt%) in srp3. For that reason, the amount of Ca leached from serpentinites was very low and below 0.5 g/kg (Fig. 1). CO_2 leaching had a stronger effect on the amount of Ca released from all serpentinite samples (srp1: 0.2 g/kg; srp2: 0.5 g/kg; srp_3: 0.9 g/kg) when compared with NH_4OAc leaches (srp_1: 0.1 g/kg; srp2: 0.2 g/kg; srp3: 0.04 g/kg). The wollastonite skarn (wol) produced leachates with twice the amount of Ca (30.0 g/kg) with the CO_2 leach when compared to the NH_4OAc leach (15.0 g/kg; Fig. 1). This sample contained 26 wt% of CaO associated with wollastonite (21.6 wt%) and diopside (41.0 wt%). More details on sample geochemistry are provided as supplementary material (Table S1). On the other hand, brucite samples (brc) had a lower CaO content (1.5 wt%) associated to dolomite (5.1 wt%), showed much less discrepancy between the two methods (0.8 mg/kg for CO_2; 0.9 mg/kg for NH_4OAc).

In general, CO_2 leaching resulted in greater Mg release than NH_4OAc leaching except for samples containing more than 10 wt% brucite (srp3, brc). An increase of 3–6 times in Mg release was observed for srp1 and srp2 when exposed to CO_2 (Fig. 1). In contrast, greater Mg release from srp3 (42.8 wt% MgO) and brc sample (62.8 wt% MgO) with NH_4OAc leaching was correlated to their high brucite content (Table 2). Brc was dominated by brucite (82.8 wt%), but also contained 6.0 wt% of hydromagnesite, 5.1 wt% dolomite, and trace amounts (<1 wt%) of pyroaurite. Mg leaching from the brucite mine sample exceeded the analytical detection limit (100 g/kg) of the NH_4OAc method. As a reference, complete dissolution of brucite in the brc sample would release 345 g/kg. On the contrary, CO_2 leaching released less Mg from the brucite mine sample, generating values ranging from 64 to 67 g/kg for replicate experiments. Similarly, Mg leaching from the Baptiste serpentinite sample (srp3), which was dominated by antigorite (78.4 wt %) and brucite (12.1 wt%), reached 40 g/kg with NH_4OAc, which equates to approximately 96% of the Mg being leached from brucite (42 g/kg). Of the three serpentinites tested, the Baptiste sample had the smallest surface area (srp3: 3.1 m^2/g, srp1: 25.3 m^2/g; srp2: 61.1 m^2/g) and showed the greatest release of cations per surface area (Fig. 2). With CO_2 leaching, 31 g/kg of Mg was leached from Baptiste serpentinite (Fig. 1). Likewise, the experiments with brcQ mixtures released 27 g/kg mostly from brucite dissolution (Fig. 1). Both srp3 and brcQ contained similar amounts of brucite. The release of Mg from the wollastonite skarn showed that less than 0.1 g/kg could be linked to the low abundances of MgO (6.4 wt%).

3.2. Cation release from Venetia mine wastes

Venetia samples had different particle size distributions and variable surface areas (Table S2). The one CRD sample analyzed was dominated by sand (73%) and pebbles (27%) with a surface area of 5.8 m^2/g. FRD samples had variable sand-to-silt ratios and a median particle diameter that ranged from 11 to 610 μm. In some cases, clays and silt were more dominant, giving rise to higher surface areas that varied from 6.5 to 12.9 m^2/g. The surface area of the pulverized DVK was 18.0 m^2/g,

Table 2
Mineral composition (wt.%) determined using XRD data and ideal chemical formulae for the different mineral feedstocks.

Minerals/ideal chemical formula				Serpentinite			Venetia kimberlite		
		Brucite mine (brc)	Wollastonite skarn (wol)	Lizard Complex (srp1)	Feather River Canyon (srp2)	Baptiste Nickel deposit (srp3)	Pulverized DVK	CRD	FRD*
Tectosilicates	Albite [$NaAlSi_3O_8$]		11.3					11.0	3.7
	Orthoclase [$KAlSi_3O_8$]		12.1					4.4	3.3
	Quartz [SiO_2]	0.2	10.7		0.8			5.5	3.1
Phyllosilicates	Antigorite [$Mg_3Si_2O_5(OH)_4$]					78.4			
	Muscovite [$KAl_2(AlSi_3O_{10}(OH,F)_2$]		0.6						
	Clinochlore [$Mg_5Al(AlSi_3O_{10})(OH)_8$]	0.5		1.4				6.8	7.0
	Lizardite [$Mg_3Si_2O_5(OH)_4$]	0.4		93.9	92.4		33.1	23.1	18.8
	Na-Smectite [$(Na,Ca)_{0.33}(Al,Mg)_2Si_4O_{10}(OH)_2{\cdot}nH_2O$]						28.1	12.3	27.0
	Phlogopite [$KAlMg_3Si_3O_{10}(OH)_2$]						16.6	7.0	9.9
	Talc [$Mg_3Si_4O_{10}(OH)_2$]							2.5	6.7
(Hydr)oxides	Brucite [$Mg(OH)_2$]	82.8			1.2	12.1			
	Hematite [Fe_2O_3]			2.4					
	Magnetite [Fe_3O_4]	2.0			4.5	3.6			
Carbonates	Calcite [$CaCO_3$]		2.8				4.4	5.2	5.2
	Dolomite [$CaMg(CO_3)_2$]	5.1							
	Hydromagnesite [$Mg_5(CO_3)_4(OH)_2{\cdot}4H_2O$]	6.0							
	Magnesite [$MgCO_3$]								
	Pyroaurite [$Mg_6Fe^{3+}_2(CO_3)(OH)_{16}{\cdot}4H_2O$]	0.6							
Nesosilicates	Forsterite [Mg_2SiO_4]	2.5		2.3	1.1	4.8			
Inosilicates	Tremolite [$Ca_2Mg_5Si_8O_{22}(OH)_2$]						2.3	9.0	6.1
	Diopside [$CaMgSi_2O_6$]		41.0			0.7	15.6	13.2	13.6
	Wollastonite [$CaSiO_3$]		21.6						
Total		100	100	100	100	100	100	100	–

*average for all FRD samples tested (n = 9).

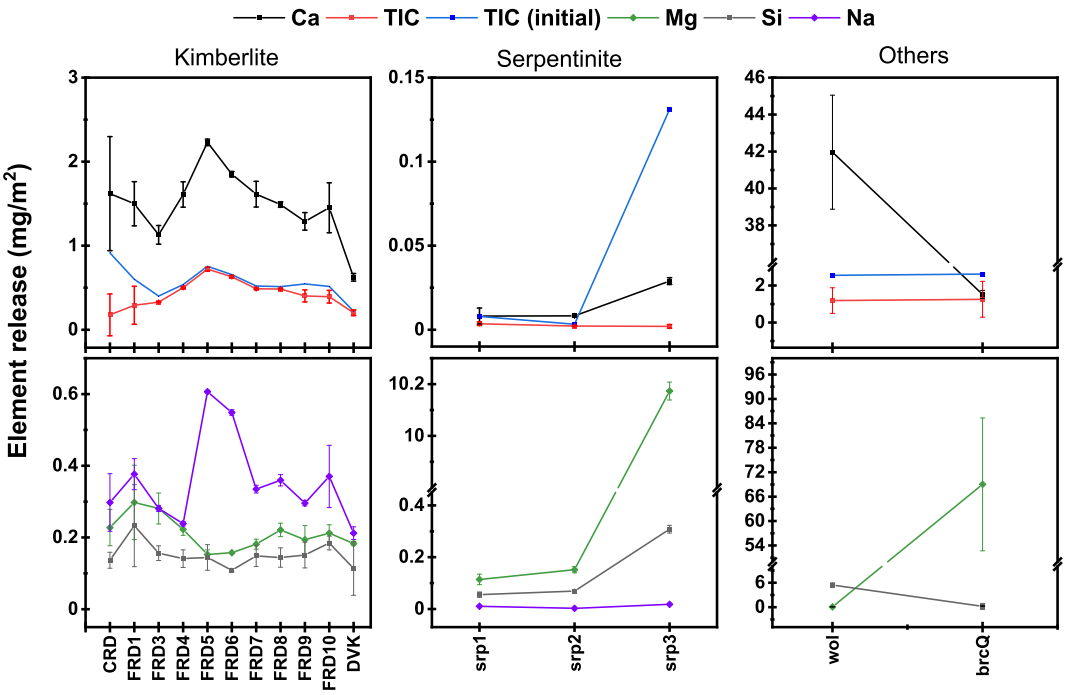

Fig. 2. Element released (Ca, Na, Mg, Si, TIC) normalized by the samples surface area in mg/m^2. Results are presented as averages (n = 3) with respective standard deviations.

which was the highest among the Venetia samples (Table 1), but still much smaller than the values measured for the two serpentinites (srp1 (25.3 m^2/g) and srp2 (61.1 m^2/g). Pulverized DVK was dominated by sand (60%), silt (35%) and contained less than 5% of clay-sized particles and a median particle diameter (d_{50}) of 171 μm (Table S2).

Both NH_4OAc and batch CO_2 leaching methods generated Ca-rich leachates from the kimberlite samples (Table 1 and Fig. 1). On average, the release of Ca from the kimberlite FRD samples and DVK was 1.4 times greater with NH_4OAc than with CO_2. In contrast, CO_2 leaching resulted in a greater release of Ca from the Venetia kimberlite CRD sample; approximately twice that of NH_4OAc leaching.

Venetia kimberlite contained less than 8 wt% of CaO (on average DVK: 7.7 wt%; FRD and CRD: 7.1 wt%). Greater calcium release was measured in FRD samples (16 g/kg with CO_2 vs. 22 g/kg with NH_4OAc), followed by DVK (11 g/kg with CO_2 vs. 19 g/kg with NH_4OAc) and CRD (9 g/kg with CO_2 vs. 4 g/kg with NH_4OAc). Calcite, diopside, tremolite, and smectite were identified as potential calcium sources in the Venetia samples (Table 2). Calcite was present at 3.8–7.0 wt% in FRD and CRD, and 4.4 wt% in DVK. Diopside content was slightly lower in CRD (~13.3 wt%) than in DVK (~15.6 wt%) and FRD (average ~13.6 wt%). Tremolite content was higher in FRD and CRD (4.0–9.0 wt%) and much lower in DVK (~2.3 wt%). The lowest smectite content was measured in CRD (~12.3 wt%), whereas the clay content in the DVK and FRD samples was much higher (18.8–30.1 wt%).

The highest MgO content in Venetia kimberlite samples was in DVK (26 wt%), whereas CRD and FRD contained 14–21 wt% MgO. Sources of Mg in Venetia kimberlite included lizardite, diopside, phlogopite, clinochlore, smectite, tremolite, and talc. DVK contained lizardite (33.1 wt %) but lesser amounts of tremolite compared to FRD and CRD (Table 2). Cation release normalized to surface area was investigated for Venetia samples (Fig. 2). Ca release from CRD was highly variable. FRD5 and FRD6, showed greater Ca released than other Venetia samples. These two samples contained more silt and clay (d_{50} < 27 μm) but surface areas similar to those measured for different FRD samples. These samples were simultaneously calcite and smectite richer than other Venetia samples (supplementary information 1). Similarly, the TIC and Na released also increased in these finer-grained samples. An opposite trend was verified for Mg and Si, where greater release of these cations was associated with the larger median diameter (d_{50} > 27 μm) feedstocks. Cation release was greater for Venetia kimberlite than for srp1 and srp2, but much less than for srp3, wol and brcQ samples which contained very reactive minerals brucite and wollastonite (Fig. 2).

3.3. Relationship between TIC, Si and easily extractable cations

TIC was measured in solids recovered from the CO_2 leachates. TIC losses in $CaCO_3$ standards represented more than 86% (Table S3) and were strongly correlated (R^2 = 0.99) to the amount of leached Ca (Fig. 3). This correlation reflects $CaCO_3$ dissolution, which was confirmed by Fourier Transform Infrared Spectroscopy (more information in the supplementary material) and showed that the characteristic wavenumbers associated with calcium carbonate were removed from spectra after CO_2 leaching.

Venetia kimberlites (calcite abundances of 3.8–7.0 wt%) showed a strong correlation between TIC and Ca released that fitted the linear trend of the $CaCO_3$ standards (R^2 = 0.99) and is consistent with the molar proportions of calcium to carbon in calcite. These observations validated the dissolution of calcite (Fig. 3a) from kimberlite. The lowest TIC change in a solid after CO_2 leaching (41% reduction) was observed for CRD, which was considerably coarser than other samples and had a relatively low surface area (5.8 m^2/g). On the other hand, carbonate dissolution (68–96% reductions in TIC; Fig. 2) was promoted in both DVK and FRD samples due their finer grain (d_{50} = 11 to 1144 μm) and the associated increase in surface area.

No relationship between the leached TIC and Ca was found for the serpentinites, and brucite samples, where Ca-carbonate minerals were either absent or in low abundance (Table 2). Moreover, no correlation between the leached TIC and Mg was found for most of the samples (Fig. 3b), apart from brcQ samples, which contained Mg-carbonates that could be a source of TIC. These carbonates included hydromagnesite, dolomite, and pyroaurite which accounted for ~12 wt% in the original brucite (brc) sample and would have been diluted in brcQ samples (Table 2). As shown in Fig. 3b, the increasing release of Mg from the brucite mine sample in the quartz matrix (brcQ) was also accompanied

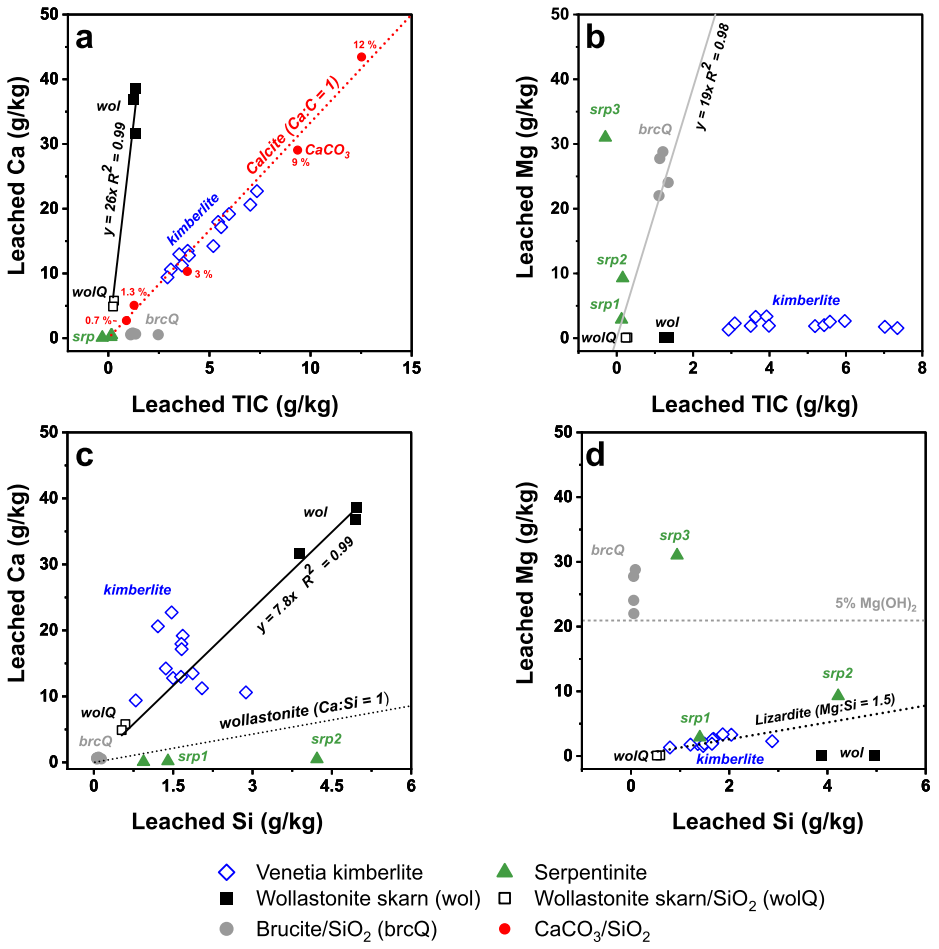

Fig. 3. Correlation analysis between the average (a) leached Ca and leached TIC, (b) leached Mg and TIC, (c) leached Ca and leached Si, and (d) leached Mg and Si for CO_2 leaching experiments. Concentration units are given as the mass of cation released per mass of the sample in g/kg. Dotted lines indicate the stoichiometric dissolution of calcite, wollastonite, and lizardite. The grey horizontal line in (d) indicate the theoretical abundance of brucite. Linear regression lines plotted for wollastonite skarn and Brucite Mine samples are indicated in (a), (b), and (c). $CaCO_3$, brucite (brcQ) and wollastonite skarn samples (wol and wolQ).

by an increase in TIC leached.

A correlation between Si and Ca release was not observed for most samples, except for the wollastonite skarn (wol and wolQ) where the concentration of both elements increased linearly for CO_2 leaching (Fig. 3c). Ca released from the serpentinites was very low and unrelated to Si release. For the serpentinites tested, srp2 had the highest (4 ± 0.4 g/kg) release of Si, and srp3 the lowest (0.9 ± 0.1 g/kg). A low amount of Si was released from brc (Fig. 3d), likely the result of serpentine or olivine dissolution. In contrast, a strong linear correlation ($R^2 = 0.94$) between the Si and Mg leached was observed for DVK, FRD, CRD, srp1, and srp2 samples (Fig. 3d). Samples containing more than 10 wt% brucite (srp3, brc, and brcQ) did not produce a correlation between the amounts of Mg and Si released.

4. Discussion

4.1. Cation release from carbonate sources during CO_2 leaching

The CO_2 batch leaching test coupled with TIC analysis was highly sensitive for detecting carbonate dissolution in CO_2 mineralization feedstocks. Results obtained from leaches using wollastonite skarn illustrate the analytical sensitivity of the method in detecting changes in TIC for samples with less than 1 wt% of inorganic carbon. The unreacted wollastonite skarn (wol) had an initial TIC abundance of 0.22 wt% and, after CO_2 leaching, only 0.08 wt% TIC remained in the solids. These results are supported by the low abundance of calcite (2.8 wt%) detected using XRD that equates to 0.34 wt% TIC. The leached TIC from wol corresponded to a variation of −0.14 wt%. This variation validates that a fraction of the easily released Ca from wollastonite skarn samples can be allocated to calcite dissolution, assuming a 1:1 M ratio of Ca to C in calcite.

A correlation between TIC and leached cations becomes even more evident in samples with greater carbonate minerals abundances. For example, leaching of Mg-carbonate sources was detected through the correlation between leached TIC and Mg (Fig. 3b) in brucite–quartz mixtures (brcQ). The abundances of hydromagnesite, dolomite, and pyroaurite in the original brucite mine (brc) sample accounted for ~12 wt% and the initial TIC was 1.22 wt% (Table 1). The batch test with brc (82.8 wt% brucite) resulted in a substantial reduction of the sample mass from 258 mg to 44 mg after leaching, for example. This change was due to the high reactivity to CO_2 since it was dominated by brucite and carbonate minerals. As a result, instead of a TIC loss, we observed an increase in TIC abundance in the solids after dissolution. The increase of TIC abundance was counterintuitive because the conditions for carbonate precipitation in liquid were not ideal (final solution pH = 6). This effect was mostly illustrated by sample brc1 (see Table S1) in that after CO_2 leaching TIC increased from 1.22% to 6.2% in the recovered solids (44 mg). Since TIC is determined as a concentration of the sample mass, a large reduction in sample mass can have a strong impact in TIC measurements. Brucite slurries (150 g of pulverized brucite mine, Nevada) exposed to 100% CO_2 were reported to have a rapid pH decline from ~9.5 to ~6.9 in 10 h and then remained in a steady-state for more than 48 h (Harrison et al., 2013). The same brucite was used in our tests, and we observed similar changes in the solution pH. In our experiments, a pH of ~9.1 was measured right after the addition of brucite samples, and at the end of the reaction with CO_2 the pH was ~5.8. Due to the rapid changes in pH, constant supply of 100% CO_2, and the low brucite mass used in our tests, it is unlikely that both brucite dissolution and carbonate precipitation occurred in our system, as observed in other studies (Harrison et al., 2013). Consequently, we interpreted the

increase in TIC as a percentage for some of the brc samples (brc1 and brc3) to be caused by complete dissolution of brucite, but incomplete dissolution of the less soluble anhydrous Mg-carbonate minerals (i.e., dolomite) that remained in the smaller sample mass following leaching.

This apparent increase in TIC will only occur if a mineral is present at a relatively high abundance and is more reactive than the carbonate minerals, thus concentrating the TIC in a much smaller recovered sample mass. The decrease in TIC abundance in the brcQ solids observed after CO_2 leaching stresses that carbonate precipitation was negligible in the CO_2-charged solution. Moreover, HCO_3^+ proton-promoted dissolution fosters brucite dissolution in mildly acidic conditions (Harrison et al., 2013; Pokrovsky et al., 2005). The dilution of this brucite-rich sample using a silica matrix helped overcome the TIC concentration effect. The experiments with brucite–quartz mixtures show a positive correlation between leached TIC and Mg ($R^2 = 0.98$; Fig. 3b), suggesting some contribution of carbonate dissolution to the amount of easily released Mg. The TIC leached from brcQ replicates (45–90% of initial TIC) resulted from Mg-carbonates dissolution, possibly of hydromagnesite which was the most abundant carbonate mineral in this sample. For comparison, the Baptiste nickel deposit sample (srp3) with 12.1 wt% brucite (cf. Power et al., 2020), showed a similar high Mg leaching (Fig. 3b). However, in this case, the Mg that was leached reflected dissolution of both brucite and Mg-silicates (serpentine) instead of Mg-carbonate dissolution as the latter phases were absent. This observation was further validated by the low TIC concentration measured in both initial and leached solids of srp3 (Table 1). The brucite–quartz mixtures had an initial TIC average of 0.11% and resulted in the loss of 0.08 wt% of TIC, validating that carbonate dissolution occurred. Theoretically, assuming that hydromagnesite dissolved and given a molar ratio of 5 Mg:4C in this mineral, the TIC leached from the sample containing 10 wt% brc and 90 wt% SiO_2 would correspond to ~0.20 wt% of Mg. Thus, it can be expected that ~2 wt% of Mg leached from the original brc samples can result from carbonate dissolution. This approach shows that even for highly reactive samples, carbonate dissolution can be identified by the TIC variation in solids.

4.2. Cation release from non-carbonate sources during CO_2 leaching of mineralogically complex samples

Relevant non-carbonate sources for easily released cations in feedstocks for CO_2 mineralization include silicates (e.g., serpentine group minerals) and hydroxides minerals (e.g., brucite) (Daval et al., 2013; Vanderzee et al., 2019). Mg leaching from silicates and hydroxides has been the focus of many reactivity studies since hydromagnesite and nesquehonite are often the desired product of *in-* and *ex-situ* CO_2 mineralization (Assima et al., 2014a; Azizi and Larachi, 2019; Harrison et al., 2013; Power et al., 2020; Thom et al., 2013; Wang and Maroto-Valer, 2011; Wilson et al., 2014). However, even at acidic pH the dissolution of Mg-silicate minerals is typically much slower than (hydr)oxide and carbonate minerals because of the stronger Si–O bonds in silicate minerals (Brantley, 2003; Oelkers, 2001; Schott et al., 2009). Although Mg-silicate minerals are widely available feedstocks, both as geological materials and industrial wastes (Baena-Moreno et al., 2019; Pan et al., 2020; Renforth, 2019; Zevenhoven et al., 2011), only a small fraction of Mg is easily extractable at low pressure and temperature conditions (Power et al., 2020; Vanderzee et al., 2019).

Previous mineral dissolution studies have shown that Mg release from serpentine minerals can be inferred from aqueous Mg/Si molar ratio (Daval et al., 2013; Power et al., 2020; Thom et al., 2013). For example, Daval et al. (2013) reported Mg/Si molar ratios between 2.5 and 2.8 for lizardite dissolution at 27 °C in the presence of HCl or CO_2. Lizardite was dominant in both the Lizard Complex (93.9 wt%) and Feather River Canyon (92.4 wt%) serpentinites and, therefore, their leach tests are comparable to those using pure serpentine minerals. The bulk Mg/Si molar ratio estimated for srp1 (Mg/Si = 2.6) and srp2 (Mg/Si = 2.4) after 48 h of the CO_2 batch leaching experiments were comparable to ratios obtained from lizardite dissolution in flow-through reactivity tests (Daval et al., 2013). The Baptiste serpentinite (srp3) showed a much higher Mg/Si ratio (~38), which is consistent with values reported by Power et al. (2020). These authors showed that the Mg/Si ratio for this serpentinite was initially very high (~30–50) due to rapid brucite dissolution and Mg detachment from serpentine surfaces within 48 h of reaction. Power et al. (2020) found also that after 72 h in flow-through dissolution experiments with the Baptiste serpentinite (srp3) the Mg/Si gradually declines to 2.5, thereby approaching stoichiometric dissolution for serpentinite [Mg:Si = 1.5, assuming an ideal formula of $Mg_3Si_2O_5(OH)_4$]. With the CO_2 batch leaching, the Mg/Si reflects the cumulative concentration of Mg in the leachates. Therefore, high Mg/Si values reflect the dissolution of highly reactive phases, which may also include carbonate minerals as well as release of surface Mg from serpentine minerals. However, the contribution of carbonates can be ruled out by combining the Mg/Si ratios with TIC analysis information. Hence, despite the limitations described above, the use of Mg/Si can serve as an indicator for the contribution of non-carbonate sources to easily extractable Mg in our batch leaching tests.

The contribution of non-carbonate sources to extractable Ca is more challenging to differentiate from leachate data, particularly when both Ca-silicate and Ca-carbonate minerals are present (e.g., wollastonite skarn; Table 2). Pure mineral studies have shown that the release of ions from wollastonite can be slowed by the partial passivation of the mineral surface with amorphous silica (Daval et al., 2009; Huijgen et al., 2006; Schott et al., 2012). Moreover, previous flow-through dissolution experiments with wollastonite indicated that steady-state dissolution under acidic conditions might only be achieved after a more prolonged exposure (3000 h) period (Schott et al., 2012). Similar behaviour has been documented for diopside (Knauss et al., 1993). Naturally, the CO_2 batch leaching presented here does not account for the factors indicated above. Therefore, we consider that using TIC analysis of the tested solids is a better alternative to extrapolate the contribution of non-carbonate sources to the easily extractable cations in the mineral feedstock.

4.3. Easily released cations from Venetia kimberlite mine wastes

The correlation between the leached TIC and leached Ca or Mg (Fig. 2) in CO_2 leaching tests can be used to infer the dissolution of carbonates. This correlation was evident in Venetia samples, with the experimental data showing a good fit to the $CaCO_3$ calibration curve ($R^2 = 0.99$). The TIC leached from Venetia samples (0.4–0.8 wt%) during CO_2 leaching was equivalent to calcite abundances of 3–7 wt%; which is comparable to those estimated from XRD analysis (~3.8–7.0 wt%; Table 2). These results provided evidence that most of the calcite dissolved during leaching.

Calcite dissolution is a spontaneous reaction under acidic conditions ($\Delta G < 0$) and is strongly regulated by the protonation of CO_3^- surface sites and formation of $>CO_3H^0$ complexation sites (Schott et al., 2009). For the full range of pH, mineral dissolution rates at ambient conditions are typically greater for calcite (10^{-10} to 10^{-7} mol/cm^2/s) than for most silicates (10^{-16} to 10^{-10} mol/cm^2/s), or even for brucite (10^{-13} to 10^{-10} mol/cm^2/s) (Brantley and Olsen, 2014; Declercq and Oelkers, 2014; Power et al., 2013a). We can assume that with constant supply and mixing of CO_2 in the batch leaching experiments, the conditions created will increase the transport of H^+ to calcium carbonate mineral surfaces prompting dissolution by surface protonation (Pokrovsky et al., 2009a). Clearly, calcite can be considered a highly reactive phase in mineral carbonation feedstocks and, for that reason, a source of easily extractable cations. From the strong correlation between leached TIC and Ca in the CO_2 batch leaching (Fig. 2a), it was concluded that most of Ca dissolved from Venetia kimberlite was linked to the dissolution of calcite.

Finer particles typically allow for greater cation release because of their high surface areas and, therefore greater exposure for aqueous carbonation (Li et al., 2018; Power et al., 2013a; Sanna et al., 2014). The effect of high surface area and fine particle size was particularly notable

for TIC leaching. Fig. 2 shows the element release from Venetia kimberlite samples normalized to surface area (mg/m^2). This relationship assumes direct proportionality between the bulk surface area and reactive surface area; yet this does not account for differing reactivities associated to mineral phases or possible changes in surface area induced by leaching or particle abrasion due to mixing during the experiment (cf. Hodson, 2006; Oelkers et al., 2018). Close to complete dissolution of TIC was noted for Venetia samples dominated by finer particles ($d_{50} < 27$ μm, FRD5, FRD6, FRD8) and with greater surface areas (>10 m^2/g) (Fig. 2; Table 1). On the contrary, TIC, Ca, Mg and Si removal from coarser samples (e.g., CRD, FRD1, FRD9, and FRD10) and smaller surface area (<10 m^2/g) showed greater variability and incomplete dissolution of TIC (Fig. 2). Mineralogically complex feedstocks that are not dominated by a single mineral phase are expected to dissolve with different kinetics and to contain surface areas with different reactivities (Dudhaiya and Santos, 2018; Hodson, 2006). These effects had more impact on samples with coarser grain size because of greater heterogeneity between replicates due to the small sample mass. Increasing the mineral-to-water ratio for coarser samples in the CO_2 leaching test may help overcome these reproducibility issues.

A potential non-carbonate source for Mg in Venetia mine residues were serpentine minerals (lizardite 12.0–33.1 wt %). Considering the Mg/Si = 1.5 for lizardite, most Venetia kimberlite residues (Fig. 3d) were aligned along a linear trend that reflects stochiometric dissolution of lizardite. Results for srp1 samples, which were mostly composed by lizardite, also fall upon this line (Fig. 2d). Serpentine dissolution may be the dominant source for Mg from Venetia kimberlites, although other sources such as diopside, clinochlore, and smectite may have also contributed.

An interesting finding of our leaches was that an increase of Na extracted was associated to samples FRD5 and FRD6 (Fig. 2) as inferred from surface area normalized data. These samples showed greater TIC and Ca leaching, and their reactivity can be linked to their greater percentages of silt- and clay-sized particles when compared to other kimberlite samples, such as DVK. Moreover, these samples contained approximately 37 wt% of smectite and ~6–7 wt% of calcite (see SI for further details). These mineral abundances were the highest measured among Venetia samples. Acid activation can promote the partial dissolution of smectites by the replacement of ions in the interchangeable layers with protons and consequent ion release (Horri et al., 2020; Komadel, 2003). This mechanism causes structural and chemical changes to smectites and is also responsible for an increase in the absorption and retention of CO_2 on the clay interlayers (Horri et al., 2020; Loring et al., 2012; Michels et al., 2015). An increase in Na released by surface area may have resulted from the extraction of Na from the smectite interlayers by CO_2. Although we cannot validate this pathway from our data, it is reasonable to assume that acid activation of smectites may have contributed to the release of cations when considering the constant supply of CO_2 gas.

4.4. CO_2 leaching versus NH_4OAc leaching

NH_4OAc leaching is a common assessment technique to determine the cation exchange capacity (CEC) of soils and targets soluble secondary minerals, carbonates, and exchangeable ions (Ciesielski et al., 1997; Dohrmann, 2006). In soils, organic acids are produced through the degradation of organics by microbes, which is often not the case in mine tailings that lack significant organic matter to promote microbial reactions (Power et al., 2014). Venetia mine residue impoundments are poor in organic carbon (<0.2 wt%) and are not expected to support significant microbial activity. For that reason, NH_4OAc leaching does not reflect the prevalent conditions in mine tailings. In this case, our CO_2 leaching tests can provide a more realistic assessment for the easily extractable cations from mineral feedstocks that are relevant to estimating the CO_2 mineralization potential under conditions where CO_2 and H_2O are the only reagents promoting dissolution.

However, the NH_4OAc method does provide complementary information about the sample reactivity. For example, there was an average increase of released Ca from kimberlite samples of 1.4 times when using the NH_4OAc leaching test (Fig. 1). In addition to carbonate dissolution, the additional Ca release was likely a result of cation-exchange reactions with the smectite clays promoted by ammonium ions (NH_4^+) (Alshameri et al., 2018; Ayari et al., 2007; Dohrmann, 2006; Zeyen et al., 2020). NH_4^+ can cause an increase of cation exchange through swelling of the smectite interlayers and consequent displacement of cations (Ca^{2+}, Mg^{2+},K^+, Na^+) onto the solution (Alshameri et al., 2018; Ayari et al., 2007). This effect was mostly observed for Venetia FRD and DVK samples, which relates to their abundance of smectite (≈28 wt%), finer grain size, and larger surface areas (6–18 m^2/g) when compared to the CRD (Table S3). NH_4OAc had a negligible effect on cation release from the serpentinites and wollastonite skarn as these did not contain smectite clays (Table 3). In fact, less Ca was extracted from the wollastonite skarn with NH_4OAc (1.4 wt%) than with CO_2 (3.5 wt%). The discrepancy suggests a limited effect of organic acids in wollastonite skarn dissolution when compared to carbonic acid. However, it is possible that the weak effect observed for NH_4OAc was due to a low concentration of organic acid that did not produce a significant effect in the dissolution of wollastonite, diopside, or smectites (cf. Golubev et al., 2006; Golubev and Pokrovsky, 2006; Pokrovsky et al., 2009b).

Samples containing more than 10 wt% brucite exhibited greater Mg release with NH_4OAc (Fig. 1), which may be due to acetate enhancing brucite dissolution as has been documented at higher concentrations (Pokrovsky et al., 2005). NH^{4+} has been used as an extracting agent for cations from mineral carbonation feedstocks in a wide range of temperatures (Guo et al., 2015; Sanna et al., 2014a; Veetil and Hitch, 2020; Wang and Maroto-Valer, 2011). The enhancement effect of NH_4OAc on brucite dissolution was further supported by the fact that CO_2 leaching released 2 to 3 times more Mg from samples without brucite, including Venetia kimberlite and serpentinites from the Lizard Complex (Table 1; Fig. 1). However, the enhancement was not observed for the Feather River Canyon (srp2) sample, which contained trace amounts of brucite (1 wt%). Identification of trace minerals by Rietveld refinement can be difficult and the error increases substantially for trace minerals abundances below 6 wt% (Raudsepp et al., 1999). Moreover, our dissolution data (Fig. 3d) suggested that Mg-silicate dissolution (i.e. serpentine) as the main source for the Mg leached from sample srp2. Most probably, the brucite content in srp2 is lower than reported and, for that reason, the predominance of brucite dissolution was negligible or undetected by our method. Previous studies showed that the extraction of Mg from silicate minerals (e.g., serpentine, forsterite) with organic acids (e.g., oxalate, acetate, citrate, EDTA, and glutamate) is limited (Bonfils et al., 2012; Declercq et al., 2013; Golubev et al., 2006; Miller et al., 2014; Ndlovu et al., 2014; Teir et al., 2007). As such, the lower Mg release with NH_4OAc when compared to CO_2 leaching is an expected outcome. Thus, despite both CO_2 and NH_4OAc showing that most of a sample's reactivity is due to the dissolution of very reactive mineral phases (i.e. carbonates and brucite), the different effects we observed in Mg leaching suggest that the NH_4OAc methodology is an imperfect predictor of the reactivity of a sample to CO_2.

Acidity is generated only by equilibrating solutions with a constant supply of pure CO_2 gas in our batch CO_2 leaching experiments. Using 100% CO_2 allows for gas solubility to be maintained during the experiments, and the capacity to mobilize the easily extractable cations from the feedstocks was maximized. Although at lower pCO_2 the release rate of cations may decrease, and carbonation reactions become less efficient, as shown by Harrison et al., (2013), the leachate compositions of the CO_2 batch-test are more consistent with mineral–CO_2 reactions than NH_4OAc and should provide a much more reliable assessment for the feedstock mineral carbonation potential at ambient conditions.

Table 3
Estimated CO_2 mineralization capacity and potential in *kg CO_2/t* for different feedstocks and the predicted GHG offset (%) for Venetia mine assuming the precipitation of easily extractable cations from non-carbonate sources.

Sample	Code	[i] Geochemistry			[ii] CO_2 batch leaching				Venetia GHGs offset*	
		CO_2 mineralization capacity in kg CO_2/t			*CO_2 mineralization potential in kg/t*					
		Mg%	**Ca%**	**CO_2**	**Mg %**	**Ca %**	**CO_2**	**CO_2 (TIC corrected)**	kt CO_2/year	**% Offset**
Brucite mine (10%brc)/SiO_2	**brcQ**	*n.d*	*n.d*	*n.d*	2.71	0.07	50	47		
Wollastonite skarn (wol)*	**wol**	3.85	18.63	274	0.01	3.62	40	36		
Serpentinites										
Lizard Complex	**srp1**	22.75	0.02	412	0.29	0.02	5	5		
Feather River Canyon	**srp2**	20.68	0.04	375	0.93	0.05	17	17		
Baptiste Nickel deposit	**srp3**	15.77	1.2	299	3.1	0.01	56	56		
Venetia kimberlite										
Dark volcanoclastic kimberlite	**DVK**	15.53	5.55	342	0.33	1.12	18	5	24	11
Coarse residue deposits	**CRD**	12.8	5.1	288	0.13	0.94	13	9	42	20
Bulk fine residue 1	**FRD1**	10.31	4.8	239	0.26	1.24	18	7	33	16
Fine residues 3	**FRD3**	13.21	4.94	293	0.34	1.35	21	7	33	16
Fine residues 4	**FRD4**	8.44	4.5	202	0.27	1.92	26	4	19	9
Fine residues 5	**FRD5**	11.52	5.07	264	0.16	2.27	28	0.8	4	2
Fine residues 6	**FRD6**	11.76	5.06	268	0.18	2.06	26	0.1	0.5	0.2
Fine residues 7	**FRD7**	9.11	4.71	217	0.2	1.8	23	3	14	7
Fine residues 8	**FRD8**	12.72	5.07	286	0.25	1.72	23	3	14	7
Fine residues 9	**FRD9**	11.94	5.78	280	0.19	1.28	18	3	14	7
Fine residues 10	**FRD10**	11.64	5.55	272	0.19	1.3	18	5	24	11

*Venetia offset calculations assume a production of 4.7 Mt of kimberlite residues per year and 210 kt of CO_2e (Mervine et al., 2018).

4.5. Estimating CO_2 mineralization potential

The total carbonation capacity of alkaline wastes can be defined as the complete conversion of its total Mg and Ca content from non-carbonate sources to carbonate products on a mole-per-mole basis (e.g., $MgCO_3$ and $CaCO_3$) (Lackner et al., 1995). However, these capacities are unlikely to be achieved at low pressure and temperature due to the sluggish dissolution rates of the silicate sources for Mg and Ca (Assima et al., 2014b; Li et al., 2018; Power et al., 2013a; Thom et al., 2013). Despite the large carbonation capacities of the serpentinites, wollastonite skarn, kimberlites, and brucite samples (200–400 kg CO_2/t; Fig. 4 and Table 3), these estimates do not account for mineral reactivity at ambient conditions. The CO_2 mineralization potential may be calculated based on the easily extractable Mg and Ca from non-carbonate sources as determined by our CO_2 batch leaching test combined with TIC analysis.

CO_2 mineralization potential estimates must account for the mineral sources that contribute to the easily extractable cations. As demonstrated by the present study, the dissolution of carbonate minerals from mineral feedstocks can be a major contributor to the pool of easily extractable cations. Carbonate dissolution is not a desirable outcome from a carbon sequestration perspective and can result in erroneously overestimating of the CO_2 mineralization potential of a feedstock. Hence, a correction factor must be included in CO_2 mineralization calculations to avoid overestimation. This factor is introduced in Equation 1 to estimate the CO_2 sequestration potential (kg CO_2/t) of a feedstock:

$$CO_2\ (kg/t) = \left[(molC_{cation} - molC_{TIC}) \times M_C\right] \times \frac{M_{CO_2}}{M_C} \times \frac{1\ g}{1000\ kg}$$

where $molC_{cation}$ are the moles of C equivalent to total leached Ca and Mg on a per tonne basis, $molC_{TIC}$ is the moles of C leached from samples on a per tonne basis, and M_C and M_{CO2} are the molar masses (g/mol) of C and CO_2, respectively. This calculation assumes a 1:1 M ratio between the

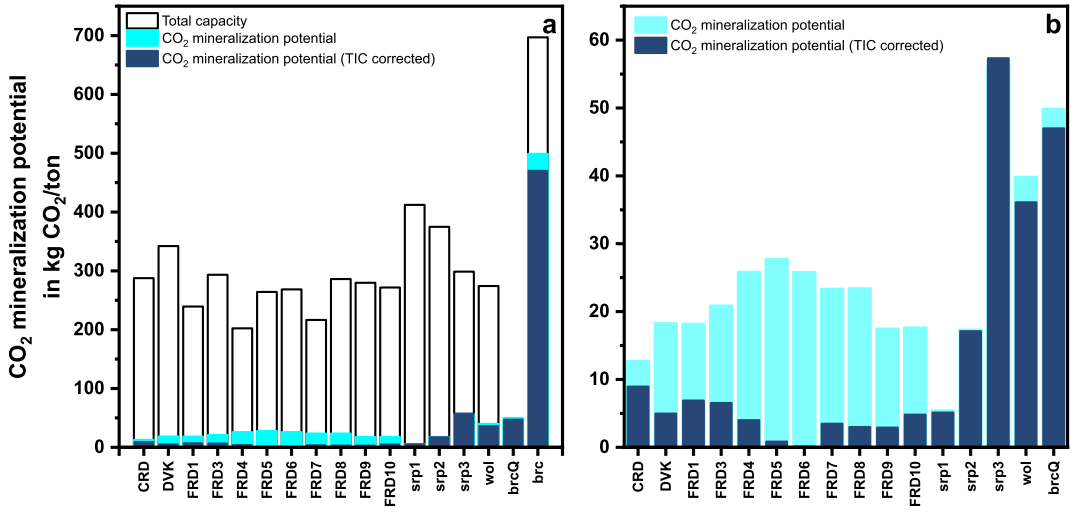

Fig. 4. Comparison between the average (a) CO_2 mineralization capacity (white) and CO_2 mineralization potential (light and dark blue) estimates based in the easily extractable cations for kimberlites, serpentinites, wollastonite skarn, and from a diluted brucite mine sample (brcQ). The corrected CO_2 mineralization potential estimates are presented in dark blue. Brc mineralization potential was extrapolated from the diluted brcQ sample. (b). Greater variations in the CO_2 mineralization potential were identified for kimberlites due to their greater carbonate content. (For interpretation of the references to color in this figure legend, the reader is referred to the Web version of this article.)

cations (Ca and Mg) and C that has the potential to be mineralized and sequestered and is corrected for the Ca and Mg that is released from carbonate sources.

Brucite and serpentine minerals are desirable sources for easily released Mg (Ding et al., 2014; Power et al., 2020; Wilson et al., 2014; Zhang et al., 2010). Brucite carbonation increases linearly with increasing pCO_2 and that promotes a fast and nearly complete dissolution of this mineral (Harrison et al., 2013). For that reason, brucite-bearing ores have greater potential for offsetting the GHG emissions of mining activities (Arce et al., 2017; Entezari Zarandi et al., 2016; Harrison et al., 2015; Power et al., 2020; Vanderzee et al., 2019; Zhao et al., 2010). The greater CO_2 mineralization potential of srp3 when compared to srp1 and srp2, for example, was proportional to its brucite content. The estimated CO_2 mineralization potential of srp3 was 55 kg CO_2/t, whereas for srp1 and srp2 was estimated at 5 and 18 kg CO_2/t, respectively. Power et al., (2020) showed that the CO_2 mineralization potential of the Baptiste serpentinite depends greatly on brucite content and varies from 20 to 90 kg CO_2/t of tailings with 0.6 and 12.6 wt% brucite (Power et al., 2020). Likewise, brucite carbonation (8.5–33.6 kg CO_2/t) was also identified as the primary driver of CO_2 mineralization at ambient conditions in the Dumont mine wastes (Quebec, Canada) with similar 11 wt% brucite and 80 wt% serpentine (Kandji et al., 2017). The majority of the easily extractable Mg from Baptiste serpentinite (srp_3 in our study) was released in the first 24 h of the dissolution with CO_2 (Power et al., 2020). Our estimates of CO_2 mineralization potential are consistent with the range determined by Power et al. (2020) for similar samples from this locality. Thus, we can conclude that the CO_2 batch leaching test can substitute for a more complex flow-through system as a methodology to quantify easily extractable cations from mineral feedstocks, provided that determination of dissolution kinetics is not required.

The rapid dissolution of brucite under high CO_2 pressure conditions generates leachates highly enriched in Mg in less than 24 h (Harrison et al., 2013; Power et al., 2020). However, under the same conditions, carbonates are also expected to dissolve. Our data show that even for a low TIC abundance (<0.5 wt%), estimates of CO_2 sequestration potential can decrease because of carbonate dissolution. For example, in brcQ the correlation between Mg and TIC indicates of carbonate dissolution in brucite-rich samples. As a result, the corrected CO_2 sequestration potential using the leached TIC (<0.1 wt%) decreased from 50 to 47 kg CO_2/t (Table 3). Clearly, greater TIC or carbonate abundance will proportionally decrease the CO_2 mineralization potential for a mineral feedstock.

Similarly, the wollastonite skarn samples had an initial TIC content 0.22 wt% and only 22 wt% wollastonite. This mineral has a simple chemical composition ($Ca_2Si_2O_6$), dissolves rapidly, and has been used as a model for Ca-rich alkaline solid residues such as steel slag (Huijgen et al., 2006; Schott et al., 2012). Based on the CO_2 batch leaching data, we estimated a CO_2 mineralization potential of approximately 36 kg CO_2/t for the wollastonite skarn (40 kg CO_2/t if not corrected with TIC). These results corroborate recent findings that showed the high potential of this wollastonite skarn as a feedstock for enhanced weathering in agricultural fields (Haque et al., 2019, 2020). However, it is important to investigate carbonate reactivity to estimate carbon budgets in ERW better. Given the examples presented, our CO_2 batch leaching method can be a valuable assessment tool to determine mineral feedstocks feasibility for CO_2 sequestration projects at ambient temperature and pressure conditions.

4.6. Implications for carbon sequestration at Venetia mine

Offsetting the annual GHG emissions (210 kt CO_{2e}/year) associated with Venetia ore production (4.7 Mt/yr) through CO_2 mineralization is currently under evaluation (Mervine et al., 2018). Complete carbonation of the Venetia kimberlite residues offers a capacity to sequester 342 kg CO_2/t residues for DVK, and 268 and 288 kg CO_2/t in FRD and CRD, respectively (Table 3 and Fig. 4). These capacities reflect the favorable chemistry of kimberlites for mineral carbonation and were comparable to those estimated for more reactive feedstocks including the wollastonite skarn and Baptiste serpentinite (Fig. 4). Complete carbonation of DVK residues, if produced at 4.7 Mt/yr, would offset 1.6 Mt CO_2/yr; however, this is unlikely to be achieved at low-temperature conditions or within the timescale of mining. A more plausible scenario would involve introducing residue management practices that enhanced the release and mineralization of the easily extractable cations within the kimberlite residues.

CO_2 leaching released on average 34% and 2% of the initial Ca and Mg in the kimberlite feedstock, respectively. Most Ca was leached from carbonate dissolution, hence an undesirable source for mineral carbonation. On the other hand, Mg leaching from kimberlite feedstocks was limited to <2% of total Mg. For comparison, 46% and 1% of the initial Ca and Mg were released with the NH_4OAc reactivity test with the increase in Ca being attributed to cation exchange with smectites. Since the CO_2 reactivity tests were performed with constant supply of CO_2, the slow kinetics of silicate dissolution will most likely be the limiting factor for CO_2 mineralization in ambient conditions at the Venetia mine.

The CO_2 mineralization potential of the Venetia kimberlite residues was determined to be 3–9 kg CO_2/t based on the release of easily extractable Ca and Mg from non-carbonate sources or 1–3% of the full carbonation capacity (Table 3). The misidentification of the cation sources results in an overestimation of approximately 300% (9–27 kg CO_2/t if not corrected with TIC). Nevertheless, 7–20% of Venetia's current GHG emissions (210 kt CO_{2e}/yr) can potentially be sequestered if the easily extractable cations are accessed for the 4.7 Mt residues generated each year (Table 3). For the FRD only, approximately 4 kg CO_2/t residues or 18,000 t CO_2/yr can be sequestered. At this rate, CO_2 mineralization would achieve an offset of 9% of Venetia emissions. Similarly, 5 kg CO_2/t residues or 23,000 t CO_2/yr could potentially be stored in the residue impoundments when DVK becomes the dominant kimberlite facies being mined, as is expected. Residue samples varied in grain size, which affected cation release and carbonate dissolution that in turn impacted CO_2 mineralization potentials. Greater carbonate dissolution associated with fine grained samples, resulted in a lower CO_2 mineralization potential (<1 kg CO_2/t). On the other hand, coarser samples with smaller surface areas, such as CRD and FRD1, showed that carbonate dissolution per surface area was much lower and, for that reason, the average mineralization potential was greater (Fig. 4). These samples, however, showed greater variation in the amount of cations released.

The fluid-to-solid ratio used in leaching tests can impact the estimation of CO_2 mineralization, as demonstrated by Kandji et al. (2017). These authors estimated that the mineral carbonation of nickel mine tailings with 11% brucite (Dumont mine, Québec, Canada) could vary from 8.5 to 33.6 kg of CO_2/t when using columns and weathering cells as kinetic leaching tests, respectively. The differences in exposed surface (0.02 cm^2/g in columns versus 1.2 cm^2/g in weathering cells), as well as the limited diffusion of CO_2 with depth in the columns were identified has the cause for lowering mineral carbonation estimates (Kandji et al., 2017). The high fluid-to-solid ratio in the CO_2 batch leaches enhances mineral dissolution and cation release, which is likely to be the rate limitation for CO_2 sequestration using Venetia residues that lack any highly reactive phases (e.g., brucite carbonation limited by CO_2 supply). Modifying residue management practices to increase the fluid-to-solid ratio such as greater areal exposure to capture more rainfall or higher use of process water may enhance mineral dissolution and thus CO_2 sequestration.

5. Conclusion

In addition to characterizing a feedstock (e.g., geochemistry, mineralogy, and physical properties), reactivity tests are needed to quantify easily extractable cations from mineralogically complex

feedstocks from non-carbonate sources under ambient conditions. Failure to exclude cations from carbonate mineral sources leads to a substantial overestimation of feedstock reactivity and CO_2 sequestration potential. Our leach test is a simple method that quantifies easily extractable cations while also distinguishing between non-carbonate (desirable) from carbonate (undesirable) cation sources and is suitable for evaluating a wide range of natural feedstocks and industrial wastes. The production of alkaline wastes is estimated to surpass 15 Gt per year by 2100, and the production of alkaline mine wastes to reach 3.5 Gt per year (Renforth, 2019). The new CO_2 batch leaching coupled with TIC analyses is a useful tool for evaluating compositionally diverse alkaline wastes for enhanced rock weathering and CO_2 mineralization.

Declaration of competing interest

The authors declare that they have no known competing financial interests or personal relationships that could have appeared to influence the work reported in this paper.

Acknowledgments

We are grateful for the funding provided by De Beers Group of Companies and support while at the Venetia Diamond Mine. Zandile Miya, Sterling Vanderzee and Evelyn Mervine are thanked for assistance with fieldwork. We are thankful to Bob Vasily from Canadian Wollastonite for providing material for the experiments. Funding was also provided by Natural Sciences and Engineering Research Council of Canada Discovery grants (RGPIN-2018-04490), a Natural Resources Canada Clean Growth grant (CGP-17-0739), and a Mitacs Accelerate grant (IT12426) to Power and Wilson.

Appendix A. Supplementary data

Supplementary data to this article can be found online at https://doi.org/10.1016/j.apgeochem.2021.104955.

References

Alshameri, A., He, H., Zhu, J., Xi, Y., Zhu, R., Ma, L., Tao, Q., 2018. Adsorption of ammonium by different natural clay minerals: characterization, kinetics and adsorption isotherms. Appl. Clay Sci. 159, 83–93.

Arce, G.L.A.F., Soares Neto, T.G., Ávila, I., Luna, C.M.R., Carvalho, J.A., 2017. Leaching optimization of mining wastes with lizardite and brucite contents for use in indirect mineral carbonation through the pH swing method. J. Clean. Prod. 141, 1324–1336.

Assima, G.P., Larachi, F., Molson, J., Beaudoin, G., 2014a. Comparative study of five Québec ultramafic mining residues for use in direct ambient carbon dioxide mineral sequestration. Chem. Eng. J. 245, 56–64.

Assima, G.P., Larachi, F., Molson, J., Beaudoin, G., 2014b. New tools for stimulating dissolution and carbonation of ultramafic mining residues. Can. J. Chem. Eng. 92, 2029–2038.

Awoh, A.S., Plante, B., Bussière, B., Mbonimpa, M., 2013. CO_2 consumption test for the quantification of the mineral carbonation potential of mine wastes. In: Canadian Géotechnical Conference. Montréal, Canada.

Ayari, F., Srasra, E., Trabelsi-Ayadi, M., 2007. Effect of exchangeable cations on the physicochemical properties of smectite. Surf. Eng. Appl. Electrochem. 43, 369–378.

Azizi, D., Larachi, F., 2019. Surface speciation of brucite dissolution in aqueous mineral carbonation: insights from density-functional theory simulations. J. Phys. Chem. 123, 889–905.

Baena-Moreno, F.M., Rodríguez-Galán, M., Vega, F., Alonso-Fariñas, B., Vilches Arenas, L.F., Navarrete, B., 2019. Carbon capture and utilization technologies: a literature review and recent advances. Energy Sources, Part A Recovery, Util. Environ. Eff. 41, 1403–1433.

Bonfils, B., Julcour-Lebigue, C., Guyot, F., Bodénan, F., Chiquet, P., Bourgeois, F., 2012. Comprehensive analysis of direct aqueous mineral carbonation using dissolution enhancing organic additives. International Journal of Greenhouse Gas Control 9, 334–346.

Brantley, S.L., 2003. 5.03 - reaction kinetics of primary rock-forming minerals under ambient conditions. In: Holland, H.D., Turekian, K.K. (Eds.), Treatise on Geochemistry. Pergamon, Oxford, pp. 73–117.

Brantley, S.L., Olsen, A.A., 2014. Reaction kinetics of primary rock-forming minerals under ambient conditions. In: Holland, H.D., Turekian, K.K. (Eds.), Treatise on Geochemistry, second ed. Elsevier, Oxford, pp. 69–113.

Brunauer, S., Emmett, P.H., Teller, E., 1938. Adsorption of gases in multimolecular layers. J. Am. Chem. Soc. 60, 309–319.

Ciesielski, H., Sterckeman, T., Santerne, M., Willery, J.P., 1997. A comparison between three methods for the determination of cation exchange capacity and exchangeable cations in soils. Agronomie 17, 9–16.

Daval, D., 2018. Carbon dioxide sequestration through silicate degradation and carbon mineralisation: promises and uncertainties. npj Materials Degradation 2, 11.

Daval, D., Hellmann, R., Martinez, I., Gangloff, S., Guyot, F., 2013. Lizardite serpentine dissolution kinetics as a function of pH and temperature, including effects of elevated pCO_2. Chem. Geol. 351, 245–256.

Daval, D., Martinez, I., Corvisier, J., Findling, N., Goffé, B., Guyot, F., 2009. Carbonation of Ca-bearing silicates, the case of wollastonite: experimental investigations and kinetic modeling. Chem. Geol. 265, 63–78.

Davis, A., Whitehead, C., Lengke, M., Collord, J., 2019. Acid–base accounting tests in combination with humidity cells help to predict waste rock behavior. Mine Water Environ. 38, 467–487.

Declercq, J., Bosc, O., Oelkers, E.H., 2013. Do organic ligands affect forsterite dissolution rates? Appl. Geochem. 39, 69–77.

Declercq, J., Oelkers, E.H., 2014. CarbFix Report 4 PHREEQC Mineral Dissolution Kinetics Database 5. Kinetics Database Compilation. Geoscience Environment, Toulouse.

Di Lorenzo, F., Ruiz-Agudo, C., Ibañez-Velasco, A., Gil-San Millán, R., Navarro, J.A.R., Ruiz-Agudo, E., Rodriguez-Navarro, C., 2018. The carbonation of wollastonite: a model reaction to test natural and biomimetic catalysts for enhanced CO_2 sequestration. Minerals 8, 209.

Ding, W., Fu, L., Ouyang, J., Yang, H., 2014. CO_2 mineral sequestration by wollastonite carbonation. Phys. Chem. Miner. 41, 489–496.

Dohrmann, R., 2006. Problems in CEC determination of calcareous clayey sediments using the ammonium acetate method. J. Plant Nutr. Soil Sci. 169, 330–334.

Dudhaiya, Aashvi, Santos, Rafael M., 2018. How characterization of particle size distribution pre- and post-reaction provides mechanistic insights into mineral carbonation. Geosciences 8 (7), 260. https://doi.org/10.3390/geosciences8070260.

Entezari Zarandi, A., Larachi, F., Beaudoin, G., Plante, B., Sciortino, M., 2016. Multivariate study of the dynamics of CO_2 reaction with brucite-rich ultramafic mine tailings. International Journal of Greenhouse Gas Control 52, 110–119.

Fajardy, M., Patrizio, P., Daggash, H.A., Mac Dowell, N., 2019. Negative emissions: priorities for Research and policy design. Frontiers in Climate 1.

Golubev, S.V., Bauer, A., Pokrovsky, O.S., 2006. Effect of pH and organic ligands on the kinetics of smectite dissolution at 25°C. Geochem. Cosmochim. Acta 70, 4436–4451.

Golubev, S.V., Pokrovsky, O.S., 2006. Experimental study of the effect of organic ligands on diopside dissolution kinetics. Chem. Geol. 235, 377–389.

Guo, H., Pei, Y., Wang, Z., Yang, Y., Wang, K., Xie, J., Liu, Y., 2015. Preparation of Mg $(OH)_2$ with caustic calcined magnesia through ammonium acetate circulation. Hydrometallurgy 152, 13–19.

Hamilton, J.L., Wilson, S.A., Morgan, B., Harrison, A.L., Turvey, C.C., Paterson, D.J., Dipple, G.M., Southam, G., 2020. Accelerating mineral carbonation in ultramafic mine tailings via direct CO2 reaction and heap leaching with potential for base metal enrichment and recovery. Econ. Geol. 115, 303–323.

Haque, F., Santos, R.M., Chiang, Y.W., 2020. CO_2 sequestration by wollastonite-amended agricultural soils – an Ontario field study. International Journal of Greenhouse Gas Control 97, 103017.

Haque, F., Santos, R.M., Dutta, A., Thimmanagari, M., Chiang, Y.W., 2019. Co-benefits of wollastonite weathering in agriculture: CO_2 sequestration and promoted plant growth. ACS Omega 4, 1425–1433.

Harrison, A.L., Dipple, G.M., Power, I.M., Mayer, K.U., 2015. Influence of surface passivation and water content on mineral reactions in unsaturated porous media: implications for brucite carbonation and CO_2 sequestration. Geochem. Cosmochim. Acta 148, 477–495.

Harrison, A.L., Power, I.M., Dipple, G.M., 2013. Accelerated carbonation of brucite in mine tailings for carbon sequestration. Environ. Sci. Technol. 47, 126–134.

Haszeldine, R.S., Flude, S., Johnson, G., Scott, V., 2018. Negative emissions technologies and carbon capture and storage to achieve the Paris Agreement commitments. Phil. Trans. Math. Phys. Eng. Sci. 376, 20160447.

Hodson, M.E., 2006. Does reactive surface area depend on grain size? Results from pH 3, 25°C far-from-equilibrium flow-through dissolution experiments on anorthite and biotite. Geochem. Cosmochim. Acta 70, 1655–1667.

Horri, N., Sanz-Pérez, E.S., Arencibia, A., Sanz, R., Frini-Srasra, N., Srasra, E., 2020. Effect of acid activation on the CO2 adsorption capacity of montmorillonite. Adsorption 26, 793–811.

Huijgen, W.J.J., Witkamp, G.-J., Comans, R.N.J., 2006. Mechanisms of aqueous wollastonite carbonation as a possible CO_2 sequestration process. Chem. Eng. Sci. 61, 4242–4251.

Inap, 2009. Global acid rock drainage guide (GARD guide). The International Network for Acid Prevention (INAP). http://www.gardguide.com. (Accessed 1 October 2019).

Ipcc, 2018. In: Masson-Delmotte, V., P, Z., Pörtner, H.O., Roberts, D., Skea, J., Shukla, P. R., Pirani, A., Moufouma-Okia, W., Péan, C., Pidcock, R., Connors, S., Matthews, J.B. R., Chen, Y., Zhou, X., Gomis, M.I., Lonnoy, E., Maycock, T., Tignor, M., Waterfield, T. (Eds.), IPCC, 2018: Global Warming of 1.5°C. An IPCC Special Report on the Impacts of Global Warming of 1.5°C above Pre-industrial Levels and Related Global Greenhouse Gas Emission Pathways, in the Context of Strengthening the Global Response to the Threat of Climate Change, Sustainable Development, and Efforts to Eradicate Poverty (in press).

Ipcc, 2019. Climate Change and Land: an IPCC special report on climate change, desertification, land degradation, sustainable land management, food security, and greenhouse gas fluxes in terrestrial ecosystems. In: Shukla, P.R., Skea, J., Calvo Buendia, E., Masson-Delmotte, V., Pörtner, H.-O., Roberts, D.C., Zhai, P., Slade, R., Connors, S., van Diemen, R., Ferrat, M., Haughey, E., Luz, S., Neogi, S., Pathak, M., Petzold, J., Portugal Pereira, J., Vyas, P., Huntley, E., Kissick, K., Belkacemi, M.,

Malley, J. (Eds.), In press.Technical Summary, in: Climate Change and Land: an IPCC Special Report on Climate Change, Desertification, Land Degradation, Sustainable Land Management, Food Security, and Greenhouse Gas Fluxes in Terrestrial Ecosystems.
Kandji, E.H.B., Plante, B., Bussière, B., Beaudoin, G., Dupont, P.-P., 2017. Kinetic testing to evaluate the mineral carbonation and metal leaching potential of ultramafic tailings: case study of the Dumont Nickel Project, Amos, Québec. Appl. Geochem. 84, 262–276.
Kirchofer, A., Brandt, A., Krevor, S., Prigiobbe, V., Becker, A., Wilcox, J., 2013. Assessing the potential of mineral carbonation with industrial alkalinity sources in the U.S. Energy Procedia 37, 5858–5869.
Knauss, K.G., Nguyen, S.N., Weed, H.C., 1993. Diopside dissolution kinetics as a function of pH, CO_2, temperature, and time. Geochem. Cosmochim. Acta 57, 285–294.
Komadel, P., 2003. Chemically modified smectites. Clay Miner. 38, 127–138.
Kremer, D., Etzold, S., Boldt, J., Blaum, P., Hahn, K.M., Wotruba, H., Telle, R., 2019. Geological mapping and characterization of possible primary input materials for the mineral sequestration of carbon dioxide in europe. Minerals 9, 485.
Lackner, K.S., Wendt, C.H., Butt, D.P., Joyce, E.L., Sharp, D.H., 1995. Carbon dioxide disposal in carbonate minerals. Energy 20, 1153–1170.
Li, J., Hitch, M., Power, I.M., Pan, Y., 2018. Integrated mineral carbonation of ultramafic mine deposits—a review. Minerals 8, 147.
Loring, J.S., Schaef, H.T., Turcu, R.V.F., Thompson, C.J., Miller, Q.R.S., Martin, P.F., Hu, J., Hoyt, D.W., Qafoku, O., Ilton, E.S., Felmy, A.R., Rosso, K.M., 2012. In situ molecular spectroscopic evidence for CO2 intercalation into montmorillonite in supercritical carbon dioxide. Langmuir 28, 7125–7128.
McCutcheon, J., Turvey, C.C., Wilson, S.A., Hamilton, J.L., Southam, G., 2017. Experimental deployment of microbial mineral carbonation at an asbestos mine: potential applications to carbon storage and tailings stabilization. Minerals 7, 191.
Mervine, E.M., Wilson, S.A., Power, I.M., Dipple, G.M., Turvey, C.C., Hamilton, J.L., Vanderzee, S., Raudsepp, M., Southam, C., Matter, J.M., Kelemen, P.B., Stiefenhofer, J., Miya, Z., Southam, G., 2018. Potential for offsetting diamond mine carbon emissions through mineral carbonation of processed kimberlite: an assessment of De Beers mine sites in South Africa and Canada. Mineral. Petrol. 112, 755–765.
Michels, L., Fossum, J.O., Rozynek, Z., Hemmen, H., Rustenberg, K., Sobas, P.A., Kalantzopoulos, G.N., Knudsen, K.D., Janek, M., Plivelic, T.S., da Silva, G.J., 2015. Intercalation and retention of carbon dioxide in a smectite clay promoted by interlayer cations. Sci. Rep. 5, 8775.
Miller, Q.R.S., Kaszuba, J.P., Schaef, H.T., Thompson, C.J., Qiu, L., Bowden, M.E., Glezakou, V.A., McGrail, B.P., 2014. Experimental study of organic ligand transport in supercritical CO_2 fluids and impacts to silicate reactivity. Energy Procedia 63, 3225–3233.
Minx, J.C., Lamb, W.F., Callaghan, M.W., Fuss, S., Hilaire, J., Creutzig, F., Amann, T., Beringer, T., de Oliveira Garcia, W., Hartmann, J., Khanna, T., Lenzi, D., Luderer, G., Nemet, G.F., Rogelj, J., Smith, P., Vicente Vicente, J.L., Wilcox, J., del Mar Zamora Dominguez, M., 2018. Negative emissions—Part 1: Research landscape and synthesis. Environ. Res. Lett. 13, 063001.
National Academies of Sciences, E., and Medicine, 2019. Negative Emissions Technologies and Reliable Sequestration: A Research Agenda.
Ndlovu, B., Morkel, J., Naudé, N., 2014. Kimberlite weathering: effects of organic reagents. Miner. Eng. 57, 68–71.
Oelkers, E.H., 2001. General kinetic description of multioxide silicate mineral and glass dissolution. Geochem. Cosmochim. Acta 65, 3703–3719.
Oelkers, E.H., Declercq, J., Saldi, G.D., Gislason, S.R., Schott, J., 2018. Olivine dissolution rates: a critical review. Chem. Geol. 500, 1–19.
Oelkers, E.H., Gislason, S.R., Matter, J., 2008. Mineral carbonation of CO2. Elements 4, 333–337.
Pan, S.-Y., Chen, Y.-H., Fan, L.-S., Kim, H., Gao, X., Ling, T.-C., Chiang, P.-C., Pei, S.-L., Gu, G., 2020. CO_2 mineralization and utilization by alkaline solid wastes for potential carbon reduction. Nature Sustainability 3, 399–405.
Parkhurst, D.L., Appelo, C.A.J., 2013. Description of input and examples for PHREEQC version 3—a computer program for speciation, batch-reaction, one-dimensional transport, and inverse geochemical calculations. U.S. Geological Survey Techniques and Methods, book 6, chap. A43, 497 p available only at. https://pubs.usgs.gov/tm/06/a43/.
Pogge von Strandmann, P.A.E., Burton, K.W., Snæbjörnsdóttir, S.O., Sigfússon, B., Aradóttir, E.S., Gunnarsson, I., Alfredsson, H.A., Mesfin, K.G., Oelkers, E.H., Gislason, S.R., 2019. Rapid CO_2 mineralisation into calcite at the CarbFix storage site quantified using calcium isotopes. Nat. Commun. 10, 1983.
Pokrovsky, O.S., Golubev, S.V., Schott, J., Castillo, A., 2009a. Calcite, dolomite and magnesite dissolution kinetics in aqueous solutions at acid to circumneutral pH, 25 to 150 °C and 1 to 55 atm pCO_2: new constraints on CO_2 sequestration in sedimentary basins. Chem. Geol. 265, 20–32.
Pokrovsky, O.S., Schott, J., Castillo, A., 2005. Kinetics of brucite dissolution at 25°C in the presence of organic and inorganic ligands and divalent metals. Geochem. Cosmochim. Acta 69, 905–918.
Pokrovsky, O.S., Shirokova, L.S., Bénézeth, P., Schott, J., Golubev, S.V., 2009b. Effect of organic ligands and heterotrophic bacteria on wollastonite dissolution kinetics. Am. J. Sci. 309, 731–772.
Power, I.M., Dipple, G.M., Bradshaw, P.M.D., Harrison, A.L., 2020. Prospects for CO_2 mineralization and enhanced weathering of ultramafic mine tailings from the Baptiste nickel deposit in British Columbia, Canada. International Journal of Greenhouse Gas Control 94, 102895.
Power, I.M., Harrison, A.L., Dipple, G.M., Wilson, S.A., Kelemen, P.B., Hitch, M., Southam, G., 2013a. Carbon mineralization: from natural analogues to engineered systems. Rev. Mineral. Geochem. 77, 305–360.
Power, I.M., McCutcheon, J., Harrison, A.L., Wilson, S.A., Dipple, G.M., Kelly, S., Southam, C., Southam, G., 2014. Strategizing carbon-neutral mines: a case for pilot projects. Minerals 4, 399–436.
Power, I.M., Wilson, S.A., Dipple, G.M., 2013b. Serpentinite carbonation for CO_2 sequestration. Elements 9, 115–121.
Raudsepp, M., Pani, E., Dipple, G.M., 1999. Measuring mineral abundance in skarn; I, the Rietveld method using X-ray powder-diffraction data. Can. Mineral. 37, 1–15.
Renforth, P., 2019. The negative emission potential of alkaline materials. Nat. Commun. 10, 1401.
Sanna, A., Lacinska, A., Styles, M., Maroto-Valer, M.M., 2014a. Silicate rock dissolution by ammonium bisulphate for pH swing mineral CO_2 sequestration. Fuel Process. Technol. 120, 128–135.
Sanna, A., Uibu, M., Caramanna, G., Kuusik, R., Maroto-Valer, M.M., 2014b. A review of mineral carbonation technologies to sequester CO_2. Chem. Soc. Rev. 43, 8049–8080.
Schott, J., Pokrovsky, O.S., Oelkers, E.H., 2009. The link between mineral dissolution/precipitation kinetics and solution chemistry. Rev. Mineral. Geochem. 70, 207–258.
Schott, J., Pokrovsky, O.S., Spalla, O., Devreux, F., Gloter, A., Mielczarski, J.A., 2012. Formation, growth and transformation of leached layers during silicate minerals dissolution: the example of wollastonite. Geochem. Cosmochim. Acta 98, 259–281.
Tait, M.A., Brown, R.J., 2008. Explosive fissure eruption of a large kimberlite pipe: Venetia K01 kimberlite pipe, Limpopo, RSA. International Kimberlite Conference. Extended Abstracts 9.
Teir, S., Revitzer, H., Eloneva, S., Fogelholm, C.-J., Zevenhoven, R., 2007. Dissolution of natural serpentinite in mineral and organic acids. Int. J. Miner. Process. 83, 36–46.
Thom, J.G.M., Dipple, G.M., Power, I.M., Harrison, A.L., 2013. Chrysotile dissolution rates: implications for carbon sequestration. Appl. Geochem. 35, 244–254.
Vanderzee, S.S.S., Dipple, G.M., Bradshaw, P.M.D., 2019. Targeting highly reactive labile magnesium in ultramafic tailings for greenhouse-gas offsets and potential tailings stabilization at the Baptiste deposit, central British Columbia (NTS 093K/13, 14). Geoscience BC Summary of Activities 2018: Minerals and Mining, Geoscience BC Report 2019-1 109–118.
Veetil, S.P., Hitch, M., 2020. Recent developments and challenges of aqueous mineral carbonation: a review. Int. J. Environ. Sci. Technol.
Wang, X., Maroto-Valer, M.M., 2011. Dissolution of serpentine using recyclable ammonium salts for CO_2 mineral carbonation. Fuel 90, 1229–1237.
Wilson, S.A., Dipple, G.M., Power, I.M., Barker, S.L., Fallon, S.J., Southam, G., 2011. Subarctic weathering of mineral wastes provides a sink for atmospheric CO(2). Environ. Sci. Technol. 45, 7727–7736.
Wilson, S.A., Harrison, A.L., Dipple, G.M., Power, I.M., Barker, S.L.L., Ulrich Mayer, K., Fallon, S.J., Raudsepp, M., Southam, G., 2014. Offsetting of CO2 emissions by air capture in mine tailings at the Mount Keith Nickel Mine, Western Australia: rates, controls and prospects for carbon neutral mining. International Journal of Greenhouse Gas Control 25, 121–140.
Zevenhoven, R., Fagerlund, J., Songok, J.K., 2011. CO_2 mineral sequestration: developments toward large-scale application. Greenhouse Gases: Sci. Technol. 1, 48–57.
Zeyen, N., Wang, B., Wilson, S.A., Von Gunten, K., Alessi, D.S., Paulo, C., Stubbs, A.R., Power, I.M., 2020. Cation Exchange: a New Strategy for Mineral Carbonation of Smectite-Rich Kimberlites. Goldschmidt2020 Abstract.
Zhang, J., Zhang, R., Geerlings, H., Bi, J., 2010. A novel indirect wollastonite carbonation route for CO_2 sequestration. Chem. Eng. Technol. 33, 1177–1183.
Zhao, L., Sang, L., Chen, J., Ji, J., Teng, H.H., 2010. Aqueous carbonation of natural brucite: relevance to CO_2 sequestration. Environ. Sci. Technol. 44, 406–411.